Semarak Engineering Journal

Journal homepage:
https://semarakilmu.my/index.php/sej/index
ISSN: 3036-0145

Numerical strategies for a full time-scale transient simulation of progressive-burning solid rocket motors' internal ballistics

Matías Quintana Rebolledo[1,*], Pablo Cornejo[1], Alejandro López-Telgie[1], César Morales-Verdejo[2,3]

[1] Departamento de Ingeniería Mecánica, Facultad de Ingeniería, Universidad de Concepción, Chile
[2] Universidad Bernardo O'Higgins, Facultad de Ciencias de la Salud, Centro Integrativo de Biología y Química Aplicada (CIBQA), General Gana 1702, Santiago, Chile
[3] Universidad Bernardo O'Higgins, Vicerrectoría Académica, Dirección General de Investigación, Innovación, Transferencia y Emprendimiento, General Gana 1670, Santiago, Chile

ARTICLE INFO

Article history:
Received 9 June 2026
Received in revised form 15 June 2026
Accepted 20 July 2026
Available online 29 July 2026

Keywords:
CFD, internal ballistics, solid rocket motor, transient simulation

ABSTRACT

Accurate prediction of internal ballistics in solid rocket motors (SRMs) is essential for reliable design but remains challenging due to the transient nature of combustion and nozzle flow. While steady-state models are computationally efficient, they fail to capture time-dependent effects such as shock wave formation. This study presents a full time-scale CFD simulation of progressive-burning sugar-based propellant, using ANSYS Fluent with both pressure-based and density-based solvers. A Realizable k–ε turbulence model with non-equilibrium wall functions and non-reactive species transport formulation was applied in a fixed-mesh approach. Simulations reproduced the complete burn time of several experimental tests. Both solvers captured shock wave dynamics consistently, but the pressure-based solver achieved convergence within 4 days, whereas a density-based solver would require 10 days. Comparisons with experimental thrust coefficient highlighted sensitivity to burn-rate data, underscoring its critical role in quantitative accuracy. The results demonstrate that pressure-based solvers provide a practical, resource-efficient strategy for iterative SRM design without compromising essential flow physics.

1. Introduction

Working with an iterative design philosophy is a common practice when using an experimental approach to solve a problem. Usually, such is the case in experimental rocketry. At the University of Concepción (UdeC), experimental rocketry has been a subject of interest since 2007, when a propulsion-oriented group (called GIP) of students was formed. Through trial and error, major breakthroughs have been achieved since its formation, but the need for more cost-effective methods to evaluate their solid rocket motor's (SRM) performance has been on the rise.

At UdeC, solid propellant grains have been manufactured to have a progressive burn. Progressive burn grains have a distinctive combustion chamber pressure behaviour, in which the pressure

* *Corresponding author.*
E-mail address: mquintana2018@udec.cl

https://doi.org/10.37934/sej.15.1.89103

continuously rises up to a maximum value. Although these types of grains need the least amount of time to manufacture, they have a major disadvantage, which is that nozzles can only be designed to fully expand the combustion products at a certain pressure (usually the average value of the curve). Outside that value, the nozzle will work at a reduced efficiency.

SRMs' performance is usually analyzed in terms of their total and specific impulse, maximum delivered thrust, or burn time, which all depend on the internal ballistics. Internal ballistics in SRMs comprise complex phenomena that tend to be heavily simplified in order to be able to model them mathematically. For instance, gas dynamics emerging from solid propellant combustion can be posed as a problem concerning only fluid dynamics or chemical reactions with or without heat transfer. Even then, the scope of the study can be further limited by analysing only the ignition transient or the formation of shock waves inside the nozzle. From the fluid dynamics perspective, the problem is usually solved by employing a chemical equilibrium program to model the solid rocket motor's combustion chamber phenomena and using some of the results from that model as input data for a CFD model of the motor's nozzle. Modelling solid rocket propellant combustion this way implies that the problem is being de-coupled, meaning that the combustion chamber and nozzle phenomena are solved separately. While doing so, the problem's difficulty and calculation time decrease drastically, but it carries along uncertainty about the effect of removing the combustion chamber from the nozzle.

Using 0-dimensional chemical equilibrium models such as NASA's CEA [15] is one way of reducing the uncertainty of this problem, and usually the fastest one at that too. Limitations arise when using chemical equilibrium models if a preview of the internal gas dynamics for nozzle or combustion chamber sizing is needed, because these models do not include accumulated effects and can only solve for specific steady-state conditions. An extended solution [17] may be suitable for preliminary design of the motor nozzle, though it will not be able to capture possible shock waves or test advanced nozzle geometries, such as bell nozzles.

Early transient and quasi-steady formulations [8,9,18,21,27] for internal ballistics aimed to tackle the problem of accumulated effects using several mathematical approximations, but they had limitations when faced against strong pressure fluctuations [8,18,21] or scarce propellant burn-rate data availability [9,27].

To solve the problem from a broader point of view, a strategy for simulating the entire burn time of a rocket motor is proposed here, limiting the created control volume to the motor's nozzle only and using only a fluid dynamics approach. Surroundings of the rocket's nozzle are not considered in the control volume in order to reduce the model's calculation time, so close attention must be paid to the boundary condition at the nozzle's exit. To the author's knowledge, there is no other work that has tried this method before, and it may be very well argued that the reason behind this is the time needed between iterations when simulating the full burn time extent of an SRM.

The scope of this paper is limited to studying the behaviour of the overall distribution of static pressure, gas density, and gas Mach number along the rocket's nozzle, without delving into the details of potential chemical reactions, heat transfer, and the influence of the nozzle geometry for shock wave formations.

1.1 Steady-state and ignition transient models

For many engineering purposes, especially in the early stages of rocket motor design, steady-state models provide sufficiently accurate predictions. Assuming steady-state removes all time-dependent terms, significantly simplifying the governing equations (mass, momentum, energy, species transport) and thus, reducing the calculation time and resource usage. The steady-state

assumption allows to isolate and study key parameters like burning rate, pressure distribution, temperature field, and heat feedback mechanisms without the complexity of transient effects [3,4,6,26]

On the other hand, transient simulations are essential to represent propellant ignition, flame extinction, and pressure oscillations (e.g., combustion instability), because phenomena such as burning front movement, erosive burning onset, and grain burnback over time cannot be captured by steady-state models [13,24,25].

In the context of progressive burn type (that is, when the static pressure in the combustion chamber behaves like a monotonically increasing function for most of the burn time), little to no information is available regarding CFD approaches, possibly because high-fidelity transient CFD simulations often require significant computational resources and time, limiting their practical application in iterative rocket design processes [22,23]. Progressive burn configurations are inherently transient, so steady-state models can only help to review some scenarios that may be important for the motor design (usually, the one where the combustion chamber reaches half of the maximum static pressure). Computational cost is of critical importance when carrying out a transient simulation. Advances in machine learning [20] may drastically increase the efficiency of computational resources, but the availability of these models is still scarce.

2. Experimental Setup

Ongoing experimental work at UdeC has revolved around *candy* propellant since its beginning, which is a heterogeneous sugar-based propellant. The oxidizer for this propellant is usually taken to be Potassium Nitrate, as it is the easiest oxidizer to acquire. The oxidizer to fuel ratio has been defined as 65/35 for all test purposes, as it is the ratio at which the propellant's performance is high, but its viscosity is not high enough to make the propellant slurry impossible to pour during its making. Though several sugar types are available, Sorbitol has been chosen as the propellant's fuel. This sugar, when combined with potassium nitrate forms the KNSB propellant, whose performance is analyzed in the chapters below.

For the testing bench, its initial configuration consisted of a steel structure that was bolted down to the floor of a container, as it is presented in figure 1. The current version of the testing bench has a Keli UDA 300 kg (±0.1 kg) shear beam load cell and a 4-20 mA 100 bar (±0.25% Full Scale precision) pressure transducer. Of all the tests carried out on this testing bench, three of them were selected initially to be compared against the simulations. Reported values of maximum pressure and thrust from these tests are shown in table 1. Figure 2 summarizes the pressure and thrust curves. No data was taken of atmospheric variables such as air temperature, humidity, wind speed, and static pressure during any of the tests.

Fig. 1. Solid rocket motors testing bench made at UdeC. Photograph not taken by the author

Table 1
Measured chamber pressure and thrust from several tests

Test	Date	Pressure (±0.025 MPa)	Thrust (±1 N)
1	20-nov-2024	10.6	1830
2	18-jun-2025	7.5	1316
3	18-jun-2025	10.2	1116

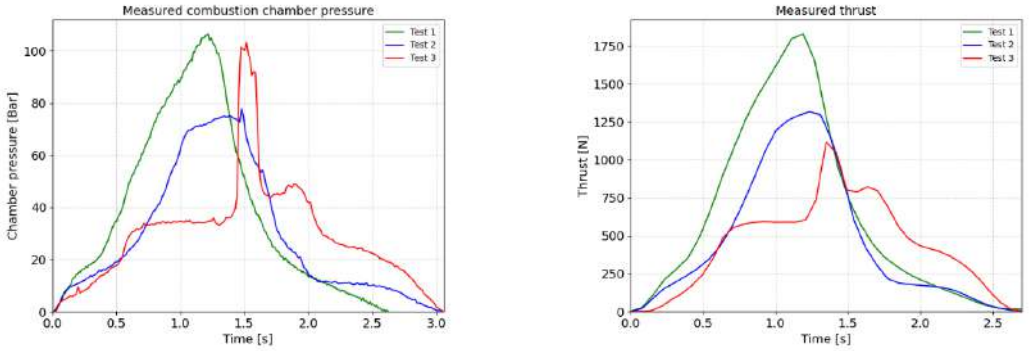

a) Chamber pressure b) Generated thrust

Fig. 2. Measured combustion chamber pressure and generated thrust of the 3 tests carried out at UdeC

2.1 A full time-scale transient approach

Transient numerical approaches to simulate the internal ballistics of SRM tend [1,5,11,19] to include turbulence in their models through the $k-\varepsilon$ formulation. Although this turbulence model has a relatively simple mathematical formulation, from an engineering standpoint, its precision is high enough to provide good estimates of the shear forces along the nozzle and, thus, the thrust generated by the motor.

Including chemical reactions is usually [3,4] done by first defining the number of steps that represent the overall kinetics of the solid propellant agents.

In this investigation, only turbulence effects were accounted for, since the addition of chemical reactions to the numerical model increases the computational time significantly, and its contribution to the preliminary design of the motor is minimal.

2.1.1 Geometry and mesh

The numerical model proposed herein comprises a 2D axisymmetric control volume of the interior of a Ballistics Evaluation Motor (BEM) designed and manufactured at the UdeC in 2018. As shown in figure 3, the control volume is relatively small, meaning that very small elements are created, which inevitably hinder the efficiency of the simulation. This is most evident at the nozzle's divergent section, where it is expected to have supersonic flow and thus a fine time resolution.

The generated mesh had 48,000 quadrilateral elements, with a minimum orthogonal quality of 0.75 and a maximum skewness of 0.4.

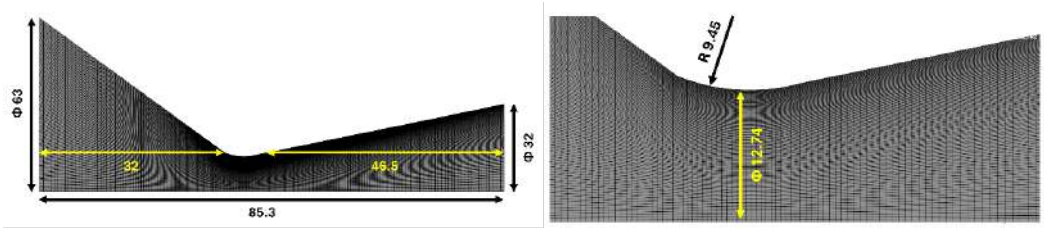

a) Nozzle dimensions and mesh b) Detail of the mesh at the nozzle's throat

Fig. 3. Generated mesh of the nozzle

2.1.2 Model configuration

A cautious analysis was carried out over ANSYS Fluent's density-based solver, as it was precise but slow enough (when compared to the pressure-based solver) to make it incompatible with an iterative design process for rocket motor nozzles. ANSYS Fluent's density-based solver solves continuity, momentum, energy, and species transport equations simultaneously, capturing the whole range of flow phenomena. In comparison, available pressure-based solvers offer at most a (pressure-based) continuity-momentum coupling, leaving energy and species transport equations to be solved after the former. Pressure-based solvers' algorithm uses the prediction-correction method [2], which is a fundamentally incompressible formulation. This method has been adapted to solve compressible flow with some drawbacks in its capability to capture shock waves adequately.

The equations solved within ANSYS Fluent's pressure-based solver are the momentum-averaged mass continuity equation (equation 1), the horizontal and vertical momentum equations with a second-order pressure interpolation scheme (equation 2, presented for the horizontal component only), the species mass fraction continuity equation (equation 3), and lastly, the energy equation (equation 4), as the combustion products were taken as if they behave like an ideal gas. Mass continuity and momentum conservation equations coupling is modelled with the Coupled scheme. Consequences of solving the whole system of equations in a segregated fashion, as is the case with pressure-based solvers [7], are: first and most importantly, a drastically lower calculation time and, in second place, a somewhat reduced precision of the static pressure distribution and fluctuations along the nozzle's axis when compared to a density-based solver. Although these weaknesses do not compromise the model's purpose, they must be seen as inherent to the nozzle design philosophy if a quick, preliminary guess of the motor's internal ballistics is needed.

$$\sum_{f}^{N_{faces}} \left[\frac{\rho_f}{2}(\vec{v}_{c_0} + \vec{v}_{c_1}) \cdot \hat{n} + J_{ho,ap} + d_f\left((p_{c_0} + (\nabla p)_{c_0} \cdot \vec{r}_0) - (\nabla p)_{c_1} \cdot \vec{r}_1\right)\right] \cdot A_f = 0 \tag{1}$$

$$a_p u = \sum_{nb} a_{nb}\, u_{nb} + \sum p_f A\hat{\imath} + S, \text{ with } p_f = \frac{1}{2}(p_{c_0} + p_{c_1}) + \frac{1}{2}(\nabla p_{c_0} \cdot \vec{r}_0 + \nabla p_{c_1} \cdot \vec{r}_1) \tag{2}$$

$$\nabla \cdot (\rho \vec{v} Y_i) = -\nabla \cdot \vec{J}_i + R_i + S_i \tag{3}$$

$$\nabla \cdot (\rho \vec{v}(h + \frac{\vec{v}^2}{2})) = \nabla \cdot (k_{eff} \nabla T - \sum_j h_j \vec{J}_j + \dot{\tau}_{eff} \cdot \vec{v}) + S_h \tag{4}$$

For the species transport model, gas products' composition is needed. This was obtained by executing NASA's CEA [15] through Python and adding KNSB to the program's propellant library. Resulting gas products' composition for a 65/35 Oxidizer/Fuel ratio is presented in table 2. Adiabatic flame temperature was also obtained the same way. For the KNSB propellant, this value is 1600 K. Thermophysical properties (e.g.: density, specific heat, thermal conductivity, viscosity, and mass diffusivity) of the gas products were set to be calculated using ideal-gas approximations, except for the mass diffusivity, which was calculated using Fluent's kinetic theory formulations. Gas composition was kept constant during the simulations as no chemical reactions are expected to happen inside the nozzle.

Table 2
Gas products composition for KNSB propellant combustion.

Product	Mole fraction [-]
CO	0.1917
CO_2	0.1762
H_2	0.1185
H_2O	0.3757
N_2	0.1378

Lastly, turbulence was included and modelled using the $k-\varepsilon$ Realizable model, which is the usual choice for these types of applications [5,11,19], as it is sufficiently robust and fast. To account for compressibility effects, there exists a specific variant of this model that modifies the Y_M term in equation 5 for $Y_M = 2\rho\varepsilon M_t^2$, where $M_t^2 = \sqrt{k/a^2}$ is the turbulent Mach number [7] and $a \equiv \sqrt{\gamma RT}$ is the speed of sound. Steady-state turbulence transport equations are presented in equations 5 and 6. Fluid-wall interactions were modelled using Non-Equilibrium Wall Functions, which enhance wall treatment of pressure gradients and are recommended when separation and reattachment of the boundary layer occur [7].

$$\frac{\partial}{\partial x_j}(\rho k u_i) = \frac{\partial}{\partial x_j}\left[\left(\mu + \frac{\mu_t}{\sigma_k}\right)\frac{\partial k}{\partial x_j}\right] + G_k + G_b - \rho\varepsilon - Y_M + S_k \tag{5}$$

$$\frac{\partial}{\partial x_i}(\rho\varepsilon u_j) = \frac{\partial}{\partial x_j}\left[\left(\mu + \frac{\mu_t}{\sigma_k}\right)\frac{\partial \varepsilon}{\partial x_j}\right] + \rho C_1 S\varepsilon - \rho C_2 \frac{\varepsilon^2}{k+\sqrt{\nu\varepsilon}} + C_{1\varepsilon}\frac{\varepsilon}{k}C_{3\varepsilon}G_b + S_\varepsilon \tag{6}$$

2.1.3 Mesh quality check

When modelling turbulence, it must be verified within the simulation that a proper y^+ value is maintained throughout the mesh. For the $k-\varepsilon$ Realizable model with non-equilibrium wall functions, the proper range of values of y^+ is between 30 and 300, as it ensures that the first element at the wall will be inside the logarithmic portion of the boundary layer. To assess the mesh size and its y^+ range, an initial steady-state simulation was run with pressure inlet and outlet boundary conditions. Pressure value at the inlet boundary was set to match test N° 1 (see table 1) value. First-order numerical schemes were employed to run the test, as they are the least accurate, thus providing a good conservative estimation of the range. The result of the test is presented in figure 4.

As can be seen from the figure, even with first-order numerical schemes, the resulting y^+values are within the proper range.

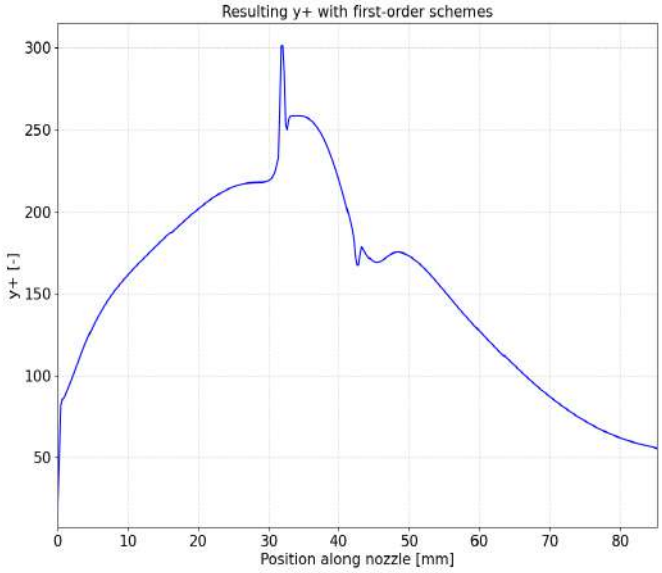

Fig. 4. y^+ values on the walls of the motor

2.1.4 Shock wave capturing accuracy

Using the same configuration as for the mesh quality check presented in the previous section, several simulations were run to analyze shock wave capturing accuracy of first order and different higher order numerical schemes available in Fluent. Results from this simulation are presented in figure 5.

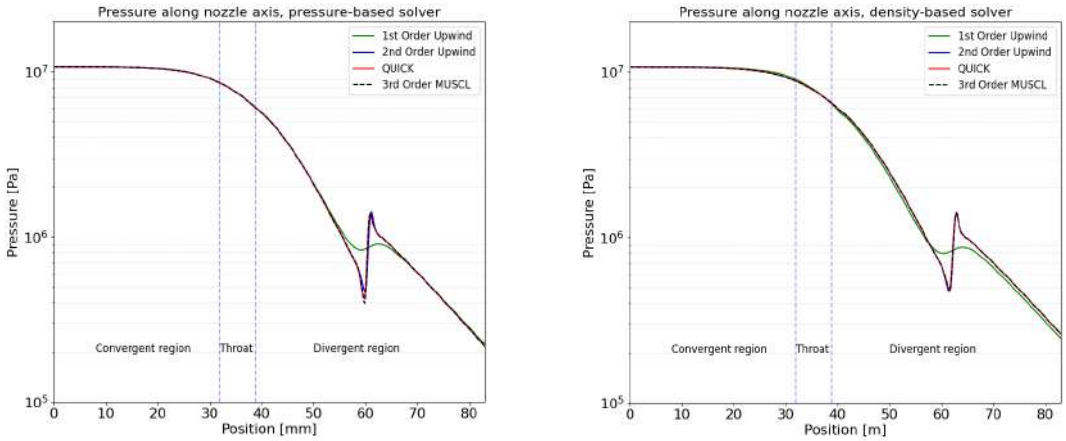

a) Pressure-based solver b) Density-based solver

Fig. 5. Pressure along the BEM's nozzle when using both solvers

The difference between both solvers is minimal in terms of accuracy but significant in terms of calculation time, as it required 5 minutes of simulation to obtain converged results using the

pressure-based solver, while the density-based solver required 11 minutes for the same number of iterations. This test was conducted with a 4-core i3-9100F processor along with 16 GB of RAM.

These simulations also provided insight into the difficulty of obtaining a solution with the density-based solver, as it seemed impossible to simulate the problem using second-order or higher numerical schemes from the beginning due to a rapid divergence of the solution. One way to sort this issue was to initialize the problem, solve 1500 iterations with first-order schemes, and then switch to higher order ones, which was not necessary at all when the pressure-based solver was being used.

From the results, it was decided to use the pressure-based solver with second-order-accurate methods, as they provided enough accuracy to capture shock waves (when compared to first-order methods, which smooth out possible discontinuities) without the downside of significantly slowing down the simulation, as would occur with QUICK or third-order MUSCL methods.

2.1.5 Boundary conditions

To avoid overdetermining the results of the simulation beforehand, a mass-flow inlet together with a pressure outlet was used. Mass flow rate corresponds to the rate of generation of gas products, and it was calculated using a simple mass conservation approach, as seen in equation 7. The steady-state, pressure-dependent burn rate (r_o) of the KNSB propellant was obtained from Nakka [17]. Mass flow rate curves are presented in figure 6. It is evident that this method delivers an approximation of the instantaneous burn rate (which depends on flame temperature, grain geometry, thermal conductivity, etc. [14], but since available data for candy propellant burn rate was not available at the time this research was conducted, this was the best method for representing it. For a more accurate, data-dependent approximation, one may use the methods developed by Ma et al. [12], which involve adding the effects of erosive burning to the steady-state formulation.

$$\dot{m}_g = \dot{m}_{burn} = \frac{\Delta m}{\Delta t} = \frac{\Delta(V_p \cdot \rho_p)}{\Delta t} \tag{7}$$

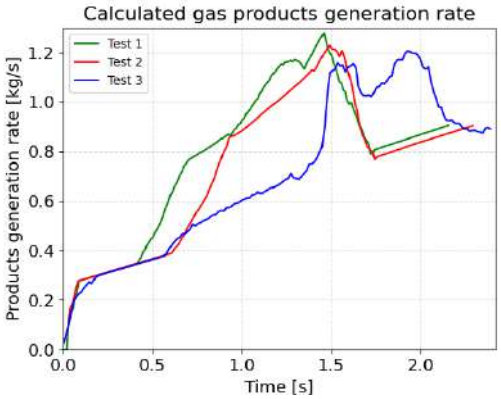

Fig. 6. Gas products generation rate obtained from pressure measurements

The mass flow rate curves presented above were loaded into Fluent by means of a transient table, which allows input of raw experimental data, avoiding any kind of approximation (like an n-order fitting) to the measured data.

As can be seen from the mass flow rate curves, the total time (horizontal axis) is different from the one presented in figure 2. The reason behind this difference is the approach that was taken

to calculate the mass flow rate. It was assumed that the solid propellant began burning at the very beginning of the tests. This, however, means that it was also assumed that there wasn't an ignition transient but an instantaneous combustion of the propellant grain. This assumption is not necessarily true, but it doesn't have any impact on the overall distribution of the flow variables, since the ignition transient occurs during the first hundredths of a second [14].

Lastly, gas products' temperature at the nozzle's inlet was set as constant, with a value of $1600\ K$. This was done to reduce the dependency on complex 1-D combustion wave calculations, which are required to have a more precise time-dependent temperature function

3. Results And Discussion

Figures below contain information about static pressure, density and Mach number distribution over the whole computation domain, using contour plots. On the other hand, line plots show the same variable's distribution along the nozzle's rotation axis (collinear with the horizontal axis). These plots are presented in their normalized form in an absolute way (e.g. values are normalized over the absolute maximum value recorded for the variable (third row plots), meaning they also coincide with the contour plots) and in a relative way (e.g. values are normalized over the maximum value for the variable on that specific instant (second row plots)). This was done to present the magnitude of the shock waves present in the divergent region of the nozzle in a clear way.
Between simulations, differences arise in the ignition transient ($t < 0.2\ s$), which is expected due to the major pressure fluctuations that occur during this period of time. After this period, gas pressure, density and Mach number behaviour is essentially the same, changing only their maximum and minimum values. A direct observation from these results is that the nozzle design behaves as if it had an inherent static pressure onset value for the formation of shock waves.

3.1 Test 1 simulation

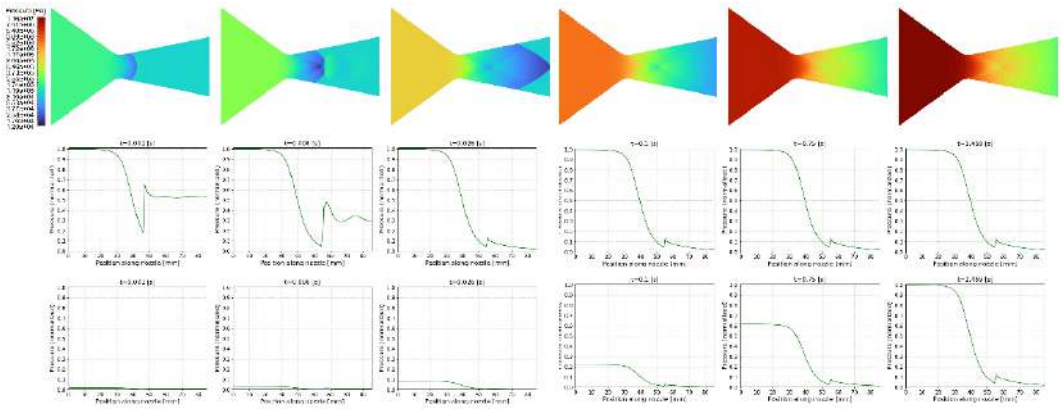

Fig. 7. *Static pressure distribution along the nozzle's axis at different flow times for simulation N 1*

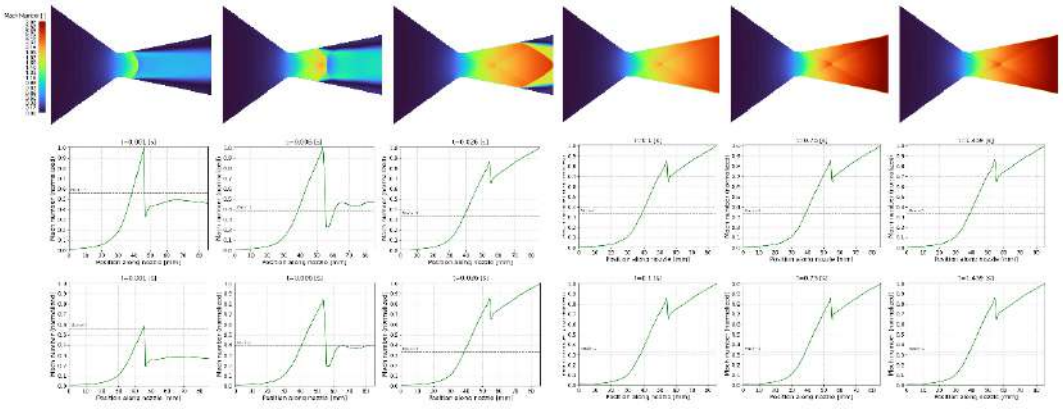

Fig. 8. Mach number distribution along the nozzle's axis at different flow times for simulation N 1

3.2 Test 2 Simulation

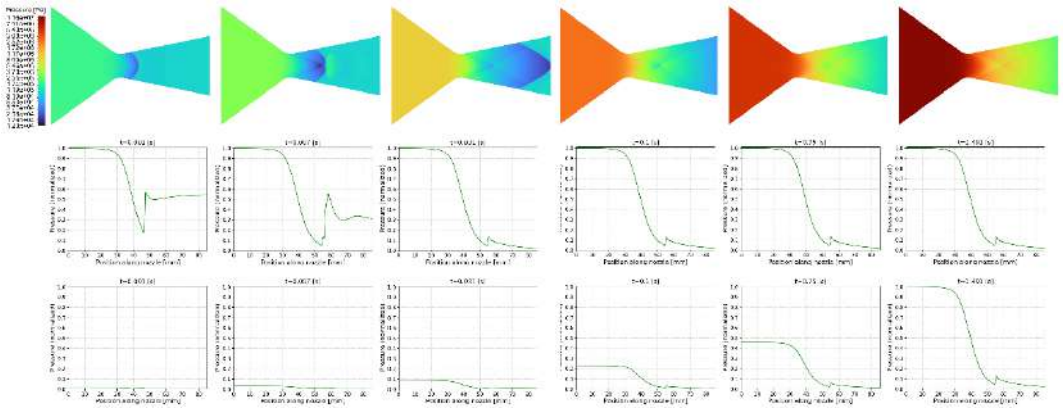

Fig. 9. Static pressure distribution along the nozzle's axis at different flow times for simulation N 2

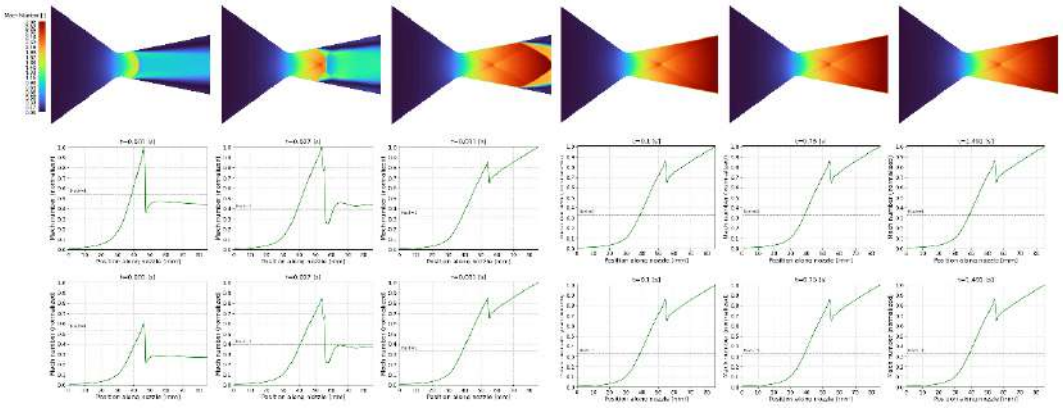

Fig. 10. Mach number distribution along the nozzle's axis at different flow times for simulation N 2

3.3 Test 3 Simulation

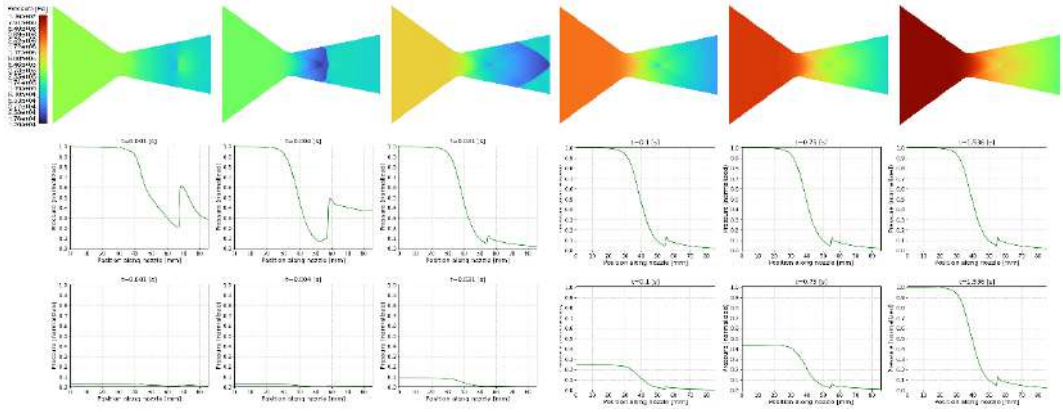

Fig. 11. Static pressure distribution along the nozzle's axis at different flow times for simulation N 3

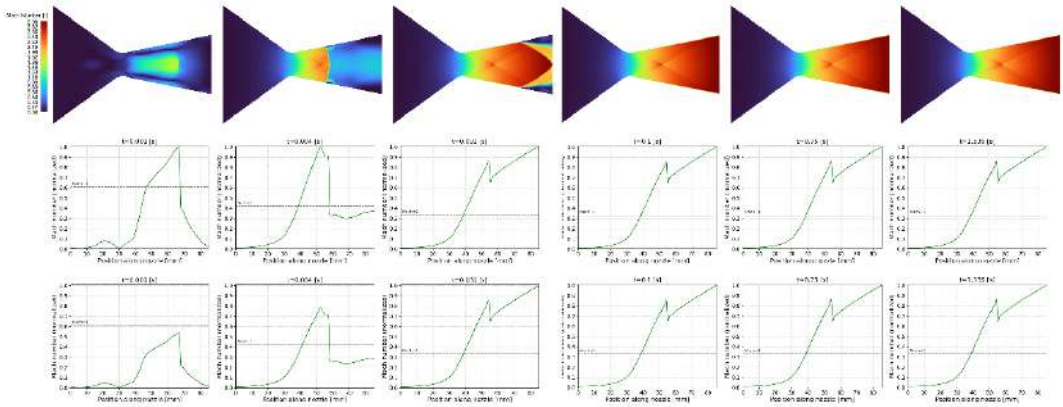

Fig. 12. Mach number distribution along the nozzle's axis at different flow times for simulation N 3

3.4 Local monitoring of variables

Figure 13 compares the thrust coefficient and characteristic velocity of the tests and their simulations. The pressure transducer and load cell sensitivity were not included in the plots, as they are negligible (see table 1). Thrust was calculated as $T = \dot{m}V_e + (p_e - p_a) \cdot A_e$, where $\dot{m}$ is the mass flow through the nozzle's exit, V_e is the gas velocity at the exit, p_e is the pressure at the exit, p_a is the ambient pressure -assumed to be 101kPa- and A_e is the nozzle's exit area, and thrust coefficient was calculated as $C_F = \frac{T}{P_C A_t}$, where T is the thrust, $\mathrm{P_C}$ is the pressure in the combustion chamber and $\mathrm{A_t}$ is the throat area. Lastly, characteristic velocity was calculated as $C^* = \frac{I_{sp} g}{C_F}$, where I_{sp} is the specific impulse, g is the gravitational acceleration (equal to 9.81 m/s^2) and C_F the thrust coefficient. The characteristic velocity was also compared against reported values from López-Telgie et al. From the results it is possible to identify a pattern related to their accuracy: for the thrust coefficient a correlation appears when its value is inside the 1.25-1.5 range. This observation shows that the way the burn rate of the propellant was approximated [17] holds relation to the real burn rate only when the thrust coefficient nears 1.5 [-], meaning that the simulated burn rate is not only higher than the experimental one, but also almost constant in magnitude.

Characteristic velocity tends to drop in magnitude in every test, but has the closest correlation to literature values in test N 1 which, coincidentally, was the closest to a purely progressive burn type.

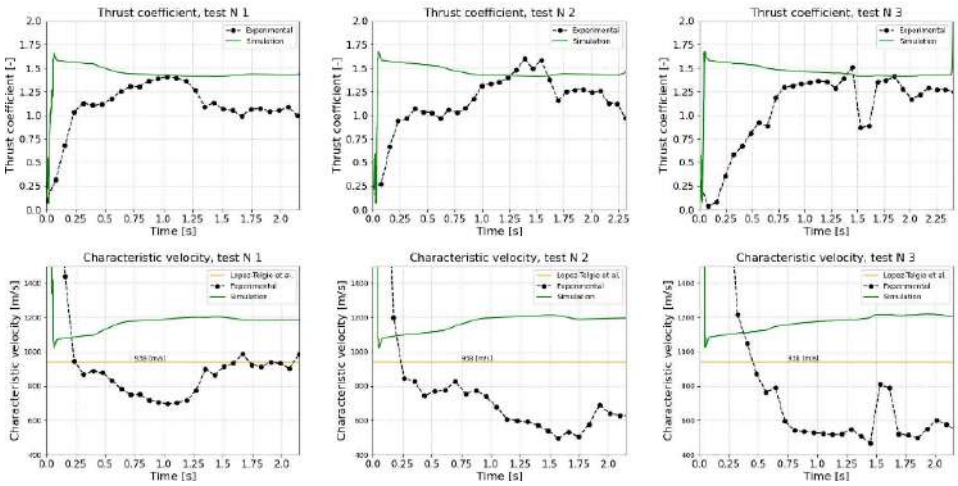

Fig. 13. Thrust coefficient (top) and characteristic velocity (bottom) from simulations and experimental

3.5 Results discussion

When comparing the simulation results of the tests, there is a noticeable difference that arises at the pseudo-ignition of the propellant, where small pressure oscillations due to the inhomogeneous burning surface significantly affect the overall pressure distribution inside the nozzle. Interest is present in noticing that the onset of shock waves appears during a similar timestamp in every test, suggesting that there is an inlet pressure threshold after which a shock wave will form, independently of the pressure history. These results are relevant and useful for the design process, as the nozzle design must consider limiting the formation of shock waves or at least dampening their effect on its efficiency.

When comparing the thrust coefficient from the simulations, however, they differ from the experimental measurements in the behaviour of the curves, though the order of magnitude of the results is correct. The differences between experimental results and simulations vary from simulation to simulation, with the most noticeable difference occurring in the simulation of the third test, where the maximum thrust coefficient from the simulation is 10.6% higher than its experimental counterpart. These differences could be attributable to the method used to calculate the generated thrust (and, thus, the coefficient), since this method differs, at most, by 10% from experimental results [16]. Checking the maximum thrust coefficient for each test and its simulation (see tables 3 and 4) allows us to see this in more detail. Maximum thrust coefficient is useful for designing the thickness of the motor and nozzle, since it is the most critical scenario from a material resistance standpoint.

Table 3
Maximum thrust coefficient comparison

	Thrust coefficient [-]		
Test	**Simulation**	**Experimental**	**Simulation difference [%]**
1	1.66	1.61	+3.1
2	1.67	1.60	+4.4
3	1.67	1.51	+10.6
Average	1.67	1.57	+6.4

Table 4
Characteristic velocity comparison (time-averaged integral)

	Characteristic velocity [m/s]		
Test	**Simulation**	**Experimental**	**Simulation difference [%]**
1	1269	1132	+12.1
2	1270	823	+54.3
3	1358	1614	-15.9
Average	3274	4123	-20.6

Differences are mostly explained by the use of a burn rate formulation developed for a specific solid propellant by Nakka [17]. This formulation should theoretically be similar to the one used in the experiments conducted for this paper, but it may not necessarily be equal, as that depends on the weather conditions (air temperature, humidity, pressure) under which the data were measured, the final geometry of the propellant grain, the maximum pressure due to the ignition charge, which walls of the grain are inhibited, and so on. Since no data was available about these topics, nor did the author have burn rate data related to the propellant used in these experiments, the best match was the available data by Nakka [17]. As a result of these assumptions, it can be concluded that having used burn rate data from an only theoretically equivalent propellant resulted noticeable differences between simulations and experimental data (up to a 10% difference between maximum thrust coefficients could have been regarded as tolerable).

Lastly, each set of results presented in the last section for each simulation were obtained after 4 days of continuous computation, which is sufficiently fast for what the time of a simulation like this is expected to take.

4. Conclusions

An assessment of numerical strategies to simulate the solid rocket motor's internal ballistics using CFD was presented in this paper. Results obtained gave insight into an albeit relatively, more time-efficient way to approach this iterative design-related problem. Shock wave capturing accuracy was reviewed using pressure-based and density-based continuity equations formulations (solvers) and several numerical schemes with different orders each. A fixed mesh approach was used to represent the nozzle as it is the simplest and quickest for any solver to calculate on. An overset mesh (2D) could also be used to represent the grain burn back inside the combustion chamber but would

require significantly more calculation time and would be limited to progressive burn type of grains only. Species transport was modeled with no reactions since they are not expected to happen inside the nozzle, and no erosive burning effects were taken into consideration for the burn rate formulation for the sake of simplicity. Erosive burning is most important during the ignition transient, which was not reviewed in this investigation due to the method employed to evaluate the grain's burn time.

The density-based solver captures shock wave onset just as accurately as the pressure-based solver but falls behind the latter in terms of computational efficiency by a significant margin. The review about Fluent's solvers and their usage to simulate solid rocket motors internal ballistics gave insight into a methodology that allows for a relatively quick assessment of the rocket's thrust coefficient, characteristic velocity and shock wave onset. From this review, a pressure-based solver with second-order accuracy was selected to carry out the simulations.

Burn rate data for the specific propellant to be studied are crucial and the main factor on which the simulation results will depend. Thus, it is deemed mandatory to have burn rate data of the specific propellant grains which are to be tested and then simulated.

Investigation conducted in this paper should be regarded as an initial step forward for the development of a precise and quick numerical strategy to simulate solid rocket motors' internal ballistics. As for future work, great benefit could come from using machine learning algorithms or physics-informed neural networks, as these tools could massively reduce the time needed to reach convergence within the simulations.

Acknowledgments

This work was supported by the National Agency for Research and Development (ANID)/scholarship Program/ EXPLORACION 13220074.

References

[1] Anil Hemanth, Varada, and Jyothi, U.S. 2020. "CFD Analysis of a Solid Propellant Retro Rocket Motor Using Ansys Fluent." *E3S Web Conf.* 184: 1054. https://doi.org/10.1051/e3sconf/202018401054.

[2] Chorin, Alexandre Joel. 1968. "Numerical Solution of the Navier-Stokes Equations." *Mathematics of Computation* 22 (104): 745–62. http://www.jstor.org/stable/2004575.

[3] Ecker, Tobias, Sebastian Karl, and Klaus Hannemann. 2017. "Modeling of Aluminum Particle Combustion in Solid Rocket Combustion Chambers." *53rd AIAA/SAE/ASEE Joint Propulsion Conference* 6. https://doi.org/10.2514/6.2017-4781.

[4] Ecker, Tobias, Sebastian Karl, and Klaus Hannemann. 2019. *Combustion Modeling in Solid Rocket Motor Plumes*. 6. https://doi.org/10.13009/EUCASS2019-79.

[5] Hsieh, Kwang-Chung, Vigor Yang, and Jesse Tseng. 1988. "Navier-Stokes Calculation of Solid-Propellant Rocket Motor Internal Flowfields." In *24th Joint Propulsion Conference*. AIAA. https://doi.org/10.2514/6.1988-3182.

[6] Hur, BK., and CB Kim. 2001. "A Steady-State Combustion Modelling of Composite Solid Propellants." *KSME International Journal* 15: 473–81. https://doi.org/10.1007/BF03185108.

[7] ANSYS Inc. 2021. *Ansys Fluent Theory Guide*. R2 ed.

[8] Krier, Herman. 1972. "Solid Propellant Burning Rate During a Pressure Transient." *Combustion Science and Technology* 5: 69–73.

[9] Krier, Herman, J. S. T'ien, W. A. Sirignano, and M. Summerfield. 1968. "Nonsteady Burning Phenomena of Solid Propellants: Theory and Experiments." *American Institute of Aeronautics and Astronautics* 6: 69–73. https://doi.org/10.2514/3.4490.

[10] López-Telgie, Alejandro, Murcia, Jhonathan and Morales-Verdejo, César. 2023. Characterization of Potassium Nitrate/Dextrose Solid Rocket Propellant Using Calorimetry. *Journal of the Chilean Chemical Society (68)/1.*

[11] Li, Zheng, and Hongjun Xiang. 2013/03. "Numerical Simulation of the Reactive Two-Phase Solid Rocket Motor Exhaust Plume." *Proceedings of the 2nd International Conference on Computer Science and Electronics Engineering (ICCSEE 2013)*, 2013/03, 1507–10. https://doi.org/10.2991/iccsee.2013.379.

[12] Ma, Yanjie, Futing Bao, Lin Lin, Yang Liu, and Weihua Hui. 2020. "A New Erosive Burning Model of Solid Propellant Based on Heat Transfer Equilibrium at Propellant Surface." *International Journal of Aerospace Engineering*.

[13] Ma, Yanjie, Mingming Zhan, Futing Bao, Lin Sun, and Ran Wei. 2021. "Numerical Simulation of Ignition Transient for Solid Rocket Motors with Large Aspect Ratio." *2021 12th International Conference on Mechanical and Aerospace Engineering (ICMAE)*, 66–71. https://doi.org/10.1109/ICMAE52228.2021.9522550.

[14] Martin Summerfield, Kenneth Kuo &. 1984. *Fundamentals of Solid-Propellant Combustion*. 3rd ed. Vol. 90. American Institute of Aeronauticsand Astronautics.

[15] McBride, Bonnie J., and Sanford Gordon. 1996. *Computer Program for Calculation of Complex Chemical Equilibrium Compositions and Applications. II: Users Manual and Program Description*. NASA.

[16] Mishra, D. P. 2017. *Fundamentals of Rocket Propulsion*. 1st ed. CRC Press.

[17] Nakka, Richard. 2023. *Solid Rocket Motor Design*. https://www.nakka-rocketry.net/softw.html#SRM.

[18] Parker, K., and M. Summerfield. 1964. "The Ignition Transient in Solid Propellant Rocket Motors." *AIAA*, ahead of print. https://doi.org/10.2514/6.1964-126.

[19] Sabnis, Jayant, Ravi Madabhushi, Howard Gibeling, and Henry McDonald. 1989. "On the Use of k-Epsilon Turbulence Model for Computation of Solid Rocket Internal Flows." In *25th Joint Propulsion Conference*. AIAA. https://doi.org/10.2514/6.1989-2558.

[20] Sun, XueQin, Yu Li, YiHong Li, et al. 2024. "Regression Transients Modeling of Solid Rocket Motor Burning Surfaces with Physics-Guided Neural Network." *Machine Learning: Science and Technology* 5 (1): 015034. https://doi.org/10.1088/2632-2153/ad2973.

[21] Von-Elbe, G. 1966. "Solid Propellant Ignition and Response of Combustion to Pressure Transients." *AIAA*, ahead of print. https://doi.org/10.2514/6.1966-668.

[22] Wang, J. C. T. 2005. "Modern SRM Ignition Transient Modeling (Part 5): Prospective Developments in CFD Simulation." *37th AIAA/ASME/SAE/ASEE Joint Propulsion Conference & Exhibit*.

[23] Wang, Zhuopu, Kairui Yu, and Yuanzhe Liu. 2024. "A Discontinuous Galerkin–Finite Element Method for the Nonlinear Unsteady Burning Rate Responses of Solid Propellants." *Aerospace* 11 (1). https://doi.org/10.3390/aerospace11010097.

[24] Weaver, John, J. E. Donald Gauthier, and Robert Stowe. 2004. "Transient Chamber Flowfield Simulation of a Rod-and-Tube Configuration Solid Rocket Motor." In *40th AIAA/ASME/SAE/ASEE Joint Propulsion Conference and Exhibit*. AIAA. https://doi.org/10.2514/6.2004-4179.

[25] Wirzberger, Hod, and Sara Yaniv. 2007. "Solid Rocket Motor Ignition Transient Phenomenom and Pressure Buildup CFD Simulation." In *43rd AIAA/ASME/SAE/ASEE Joint Propulsion Conference & Exhibit*. AIAA. https://doi.org/10.2514/6.2007-5795.

[26] Yang, Liu, Gao Yonggang, Zhu Pengfei, Zou Yuxuan, and Dong Zhichao. 2022. "Study on Heat Transfer Model of Roughness Wall in Supersonic Two-Phase Flow of Solid Rocket Motor." *International Communications in Heat and Mass Transfer* 138. https://doi.org/https://doi.org/10.1016/j.icheatmasstransfer.2022.106319.

[27] Zel'dovich, Ya. 1964. "On a Burning Rate Under Nonsteady Pressure." *Journal of Applied Mechanics and Technical Physics* 3: 126–38.